Future Energy
Open Access Journal
ISSN 2832-0328

May 2023| Volume 02 | Issue 01 | Pages 21-28

Journal homepage: https://fupubco.com/fuen

https://doi.org/10.55670/fpll.fuen.2.2.3

Future Publishing LLC

Article

Experimental investigation on the power generation for a hexacopter using a hydrogen fuel cell stack

Gerardo Urdaneta[1*], Jacob Crawford[2], Andres Dewendt[2], Zuhanee Khan[1], Kyle McMillan[1], Christopher Meyers[1], Mohammad Sanjari[3]

[1]Department of Mechanical Engineering, Arkansas Tech University, 1811 N Boulder Ave, Russellville, AR, 72801, USA
[2]Department of Electrical Engineering, Arkansas Tech University, 1811 N Boulder Ave, Russellville, AR, 72801, USA
[3]Department of Computer Science, Arkansas Tech University, 1811 N Boulder Ave, Russellville, AR, 72801, USA

ARTICLE INFO

Article history:
Received 12 October 2022
Received in revised form
22 November 2022
Accepted 28 November 2022

Keywords:
Fuel Cell, Polymer Electrolyte Membrane,
Light Detection, and Ranging,
Lithium-Polymer Batteries

*Corresponding author
Email address:
gerar4406@gmail.com

DOI: 10.55670/fpll.fuen.2.2.3

ABSTRACT

Copter drone use has been on a steady increase over the last couple of decades. The main obstacle that has slowed down the widespread use of these systems is the limited flight time. This research paper will focus on implementing a hybrid system that includes a hydrogen fuel cell (HFC) along with a battery in a hex-copter configuration to determine its effectiveness and if possible, increase its flight time. Additionally, the different projects and studies that can be performed by students with this system were also discussed. The reason for the use of hydrogen relies on the fact that it has a higher energy density (120 kJ/g) than commercial lithium-ion polymer batteries (Li-Po), the type of batteries most commercial drones currently use, which only have an energy density of 1 kJ/g. This article was divided into two main experiments for its completion: testing the HFC and batteries with a parallel circuit composed of lightbulbs and testing both the HFC and LiPo batteries on the drone by spinning the motors without propellers. The data used for the analysis of the performance of the drone was the power drawn over the duration of each test. In addition, the fuel cell temperature and IV/IP curves were also studied. The results show a delay of less than 1 second between the transition from the fuel cell power to battery power. Additionally, it was found that both fuel cell and battery supplied energy at the same time, but the latter was almost negligible when the HFC was operating. However, the battery effectively supplied the drone with almost the same amount of power as the fuel cell when hydrogen was exhausted. Finally, it was found that the battery system plays an important role when the fuel cell is being turned on or off.

1. Introduction

During the past two decades, there has been an increase in the use of unmanned aerial vehicles for communication, delivery of products, and transportation. Aerial entertainment for the movie industry, photography, precision agriculture, and law enforcement are some of the many industries drones are currently used in [1]. Drones are being used for military purposes in extensive missions [2]. Drones can also be employed to survey roads, inspect infrastructure projects, and scan bridges for failure points in conditions where remote access is crucial. Container and tower cranes could be easily accessible by drones to be inspected, reducing the probability of accidents and injuries. The agricultural industry can also employ the drone for precision farming by outfitting a spraying system for autonomous pesticide spraying, mounting a camera to track livestock, configuring Light Detection and Ranging (LIDAR) to map the terrain for crop fields, and structure planning [3]. As a general overview, most drones are designed with Lithium-Polymer (Li-Po) batteries because of their easy accessibility and lower price. The low energy density found in batteries drastically reduces the drone's flying time [1,4]. Furthermore, due to their limited power output, batteries may limit drones when having to perform fast response maneuvers [1]. For longer flights, hydrogen fuel cells (HFCs) can be employed due to their higher power density, excellent output power, and high

efficiencies (around 50%). Due to these facts, fuel cell flight times can range between 5 to 25 hours for fixed-wing drones [2,5]. One of the reasons for their high efficiency is the fact that they can operate at high or low temperatures without any notable change in their performance [6]. Despite the many advantages HFC drones provide, they also possess disadvantages. Firstly, hydrogen fuel cells have expensive and extensive hardware [2,5]. Secondly, hydrogen also poses a problem in terms of storage. Using hydrogen as a fuel for drones also brings some risk factors since hydrogen is considered volatile under certain circumstances. Both Li-Po batteries and HFC have their merits and drawbacks; thus, if a hybrid system were to be utilized by combining both types of energy sources, one could achieve higher performance. Having Li-Po batteries to support the HFCs when they cannot provide enough power for drones, or the hydrogen is exhausted would create insurance that would also allow for longer and safer flights. Thus, in this paper, a hybrid system using two Max Amps 5s 3250mAh Li-Po batteries and the HES Aerostak A-1000 (HV) Polymer Electrolyte Membrane (PEM) fuel cell was analyzed. The objective of the present study was to determine the power-time behavior of the HES PEM fuel cell coupled with two Li-Po batteries for different loads. In addition, the temperature over time was studied as well as the current-voltage and current-power curves. Two different ground tests were employed, one using lightbulbs and another coupling the power system to the drone to test its motors. The reason for this was to determine whether the hexacopter drone could use a hybrid system involving HFC and batteries and to investigate the possibility of increasing the range and flight time by analyzing the drone power consumption and the HFC performance. The design of the drone leaned towards a larger size of approximately 1.5 m in diameter and a height of 0.4 m. The reason behind this focus is due to the lack of extensive literature regarding larger drones employing hybrid systems. The drone applications will be centered on infrastructure inspection; therefore, it must be capable of flying for extensive hours. Furthermore, the drone must be easy to control, maneuver, and environmentally/user safe. Once the fuel is exhausted, it must be capable of working with a backup battery, or if the drone requires more power than the HFC can produce, then the batteries must be able to supply that demand. Thus, lag and other power supply delays must be diligently studied.

2. System Components

The drone is constructed in a hexagonal X structure capable of maximizing flight times while keeping high stability. The drone is equipped with 6 U8II Lite KV100 brushless DC motors and 6x60 amp 12s electronic speed controllers. The power supply comes from a 1.1kW PEM fuel cell and two 3250mAh Li-Po batteries as an emergency power backup. A carbon fiber chassis was chosen to maximize the weight-to-strength ratio and improve aerodynamics. Acrylonitrile Butadiene Styrene (ABS) mounts created with a Fused Deposition Modeling (FDM) 3D printer are used for additional components such as mounting for the flight stack, Hydrogen fuel tank, and the fuel cell itself. A picture of the drone can be seen in Figure 1. Table 1 (Appendix I) shows a more in-detail description of the components used, their manufacturers, and their weights. The total weight of the system approximately amounts to 9.13 kg with an empty tank and with hydrogen stored; depending on the pressure, it can over 9.16 kg. For the drone's inner workings, there are many parts to it, and they must all work in conjunction with each other to achieve flight. The most important part of the drone is the flight controller. The flight controller receives and executes commands from the ground. On the ground, there are two devices used to communicate with the drone. There is the ground station and the radio transmitter. The transmitter is used to send direct flight commands to the flight controller via a 2.4gHz radio signal that is read by an onboard receiver that then sends the signal to the flight controller. Working with the transmitter is the ground station. There are many different options of ground stations to choose from, but the two most common are Ardupilot Mission Planner and QGroundControl. The ground station is used to monitor the flight system and to execute pre-mapped flight plans. The ground station communicates via a low frequency 915 MHz radio system. Each arm of the drone has a brushless motor and an electronic speed controller (ESC). The flight controller sends a signal to the ESC through pulse width modulation. The ESC then controls the speed of the motor. The drone is in a hexacopter configuration and spins 28" carbon fiber propellers. Due to the large propellers and having 6 motors, the drone has a theoretical power consumption of 786.9W at hover. Finally, the fuel cell and LiPo batteries work together to power the whole system. They are connected to the motherboard, and the HFC will supply the power the drone needs if there is hydrogen in the tank. If the hydrogen runs out or the power required is higher than what the HFC can supply, the batteries will provide the extra power needed.

Figure 1. Hexacopter drone

3. Experimental Setup

The lightbulbs in every test carried out were arranged in a parallel circuit, as seen in Figure 2 and Figure 3, meaning that all lightbulbs would have the same voltage across them. This arrangement was chosen to maximize the power consumption in the circuit. If a series configuration had been chosen, the overall power consumption would have decreased since this type of circuit would result in a much larger resistance when compared to a parallel configuration. The reason behind maximizing the power consumption was to create a high-demand environment for the hydrogen fuel cell, thus testing its capabilities before proceeding to flight

tests. During each test, the number of active lightbulbs gradually changed.

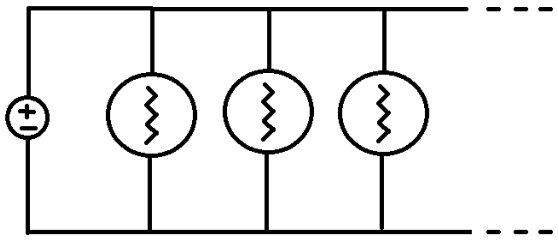

Figure 2. General schematic of parallel circuit design for lightbulb Test stand

Figure 3. Lightbulb Test 2 setup

Several experimental tests have been conducted to assess the compatibility and effectiveness of the hydrogen fuel cell (HFC) as well as the integrated system combining the hexacopter and the HFC-battery configuration. To evaluate the capability of the HFC to deliver power for varied loads, three tests were carried out using lightbulbs. The maximum number of lightbulbs used was 3 (Figure 4), 10 (Figure 5), 18 (Figure 6), and 10 (Figure 7), respectively. The power-time response was recorded for each case. Figure 4 shows the first test that was performed on the FC-battery system. Since it was the first assessment, no specific order was chosen to increase or decrease the power consumption (turn lightbulbs on and off). The total duration of the test was also arbitrary, lasting up to 1000 seconds. After enough data was collected, all three lightbulbs were turned off, and the experiment was finished. For the second experiment, shown in Figure 5, after turning on the first lightbulb 60 seconds would pass before switching on the next one. This trend would last up until the tenth lightbulb, where the system was constricted to a steady-state condition to obtain more data at higher power levels. The only exception to this was when going from 0 to 1 lightbulb since some time was needed to finalize the setup of the experiment. At the tenth lightbulb, after 300 seconds, the power was decreased by switching off one lightbulb at a time, following the same 60-second trend used in the first phase of the experiment. When the eighth lightbulb was reached, the hydrogen ran out, and the battery started supplying power. After this happened, 2 more lightbulbs were turned off, and the experiment ended because the fuel cell stopped recording data. The third test, presented in Figure 6, a similar structure to that of the previous experiment, was followed. However, 18 lightbulbs were used instead of 10, and each subsequent lightbulb was powered up after 30 seconds of turning on the previous one. The only difference in the third test was a jump from 18 lightbulbs to 17, and back to 18 since it was desired to observe the reaction of the system to fast-changing situations. Finally, after about 400 seconds in the 17-18 lightbulb range, the hydrogen ran out, 3 lightbulbs were turned off, and the experiment ended. Lastly, the fourth experiment, shown in Figure 7, was used to show the HFC-to-battery behavior for a constant load. 10 lightbulbs were turned on, and after an arbitrary amount of time (~380 s), the hydrogen valve was closed to simulate a situation where the tank ran out of hydrogen, and the transition between HFC and batteries was recorded. By briefly looking at each of the three graphs (Figures 4,5, 6, and 7), it is possible to observe that the total energy used in these experiments can be determined by obtaining the area under the curve for all three tests and adding them up. It is possible to assume that this energy will be directly dependent on the amount of hydrogen present in the tank. The batteries would also play a role in this number, but since the fuel cell would stop recording data when the hydrogen runs out, a new way must be devised to collect data after this happens. After the lightbulb tests, the HFC system was integrated with the hexacopter to carry out a motor spinning test to evaluate its operational consistency and power delivery to the drone. During the test, all 6 motors of the drone were spun with varying intensities. The motors did not have the propellers set up because this test was carried out inside the laboratory. The activity of the power consumed by the motors can be seen in Figure 8 as a function of time. From this figure, four main spikes can be seen at ~70 s, ~90 s, ~130 s, and 340 s. They can be explained by a sudden increase in the motor's throttle to ~48%, ~54%, 100%, and ~17%, respectively. It is important to know that, unlike the lightbulb tests, a maintained throttle at a high-power level approach was not pursued because the spin of the motors without propellers would have been detrimental to the drone's performance. That is why the spike approach was opted for instead. An estimation of the hydrogen energy density was obtained through the Ideal Gas Law (IGL), to compare it to the theoretical value found in the literature (low heating value). The way this was achieved was by obtaining the total power dissipated from the tests that were performed and calculating the mass flow rate by using the IGL. The Ideal Gas Law for mass flow rate can be expressed as:

$$P\dot{V} = \dot{m}RT \quad (1)$$

Where "P" is the pressure, "$\dot{V}$" is the volumetric flow rate, "$\dot{m}$" is the mass flow rate, "R" is the Universal Gas Constant, and "T" is the temperature. Lastly, the average power delivered to each lightbulb and their standard deviations were plotted in Figure 9 and Figure 10, respectively. The current-voltage (IV) and current-power (IP) curves from Test 3 were graphed in Figure 11. It is worth noting that the test data gathered after the hydrogen ran out was not used for these curves since the main power source were the batteries and not the fuel cell. In addition, data from H3 Dynamics LLC was used for comparison. Furthermore, the temperature inside the stack was measured during Test 3 in four different locations within the HFC stack. Figure 12 shows the temperature recorded by

these four sensors during Test 3 and power as a function of time, while Figure 13 shows the recorded temperatures and fan speed as a function of time.

4. Results and Discussion

The obtained data from the lightbulb tests showed a mild fluctuation in power supply for a fixed number of lightbulbs, but the variations increased in magnitude as the number of lightbulbs increased. Table 1 and Figure 9 show the combined average power supplied as a function of the number of lightbulbs. Table 1 also shows the average energy used for each number of lightbulbs for the first three tests combined. By adding all the values in the last column of Table 1 the total energy used in all three experiments can be found. This is also equivalent to taking the integral for figures 4, 5, and 6, and adding them up. The total energy used turned out to be about 1050 kJ. When divided by the 32.3 grams of hydrogen used, the energy density results in 32.5 kJ/g. The mass was calculated using the Ideal Gas Equation, since the HFC input pressure range (0.73 bar), volumetric flow rate (11 L/min), total time (3062 s), and temperature (~30 C°) were known. Thus, the mass flow rate turns out to be 0.0105 g/s, which when multiplied by the total time (3062 s) an estimate for the hydrogen used in all three tests is obtained (32.3 grams). The deviation from the actual energy density presented in the literature (120 kJ) can be explained by considering the efficiency of the fuel cell (~56%) and using the time as well as the power values when the battery was turned on [7,8]. It is also important to note that another approach that could help reduce the error can be achieved by simply measuring the mass of the tank before and after each experiment, which would yield an actual value for the mass of the hydrogen present in the tank, not simply an estimation [9].

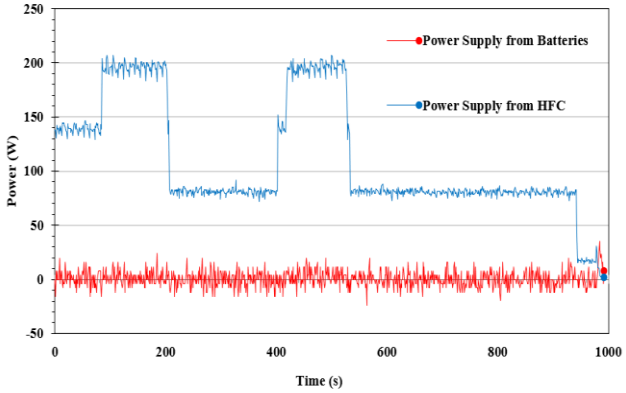

Figure 4. Power supply from HFC and batteries during lightbulb Test 1

Despite the increased range of variability at higher power levels, the general trend of total power delivered by both HFC, and batteries closely followed a linear trend, as depicted in Figure 9. The standard deviation of the total and HFC-only power delivered was calculated as a function of the power as shown in Figure 10. This figure also illustrates that the standard deviation for both cases increase with the load, explaining the steeper peaks and valleys shown in figures 4,5, 6, and 7 for higher amounts of lightbulbs (higher power delivered). Furthermore, when compared to its HFC counterpart, the smaller slope for the "Total Power Delivered line" in Figure 10 would explain how the batteries help to reduce this variability. Therefore, it can be concluded that the load draws energy from both sources and that when there is an energy surplus, the batteries get recharged (negative power values in figures 4-8).

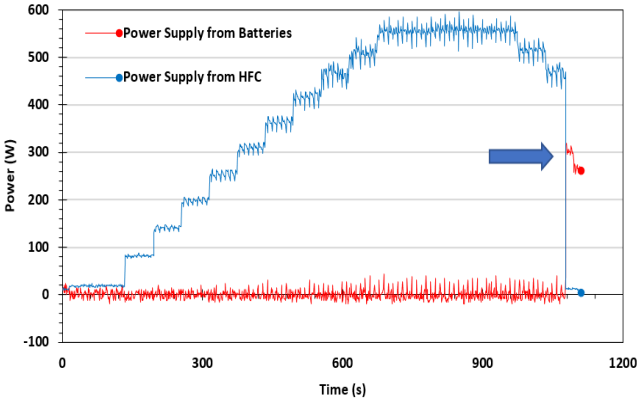

Figure 5. Power Supply from HFC and Batteries During Lightbulb Test 2

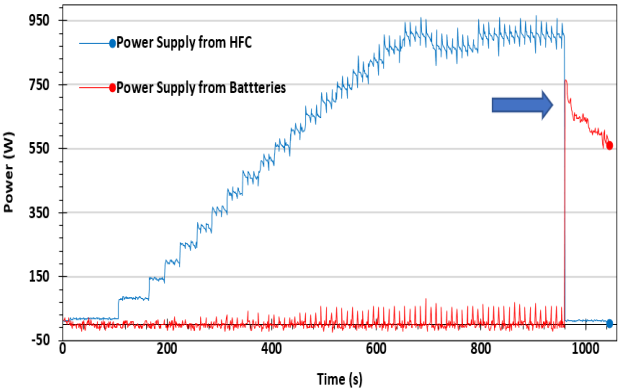

Figure 6. Power supply from HFC and batteries during lightbulb Test 3

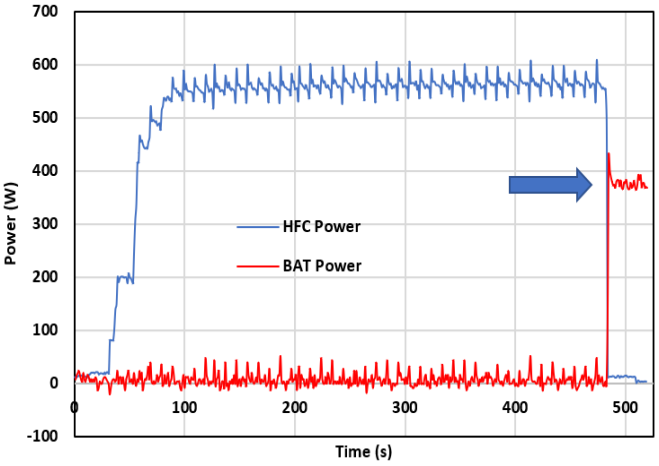

Figure 7. Power supply from HFC and batteries during lightbulb Test 4

Table 1. Combined mean power and average energy used for lightbulb Tests 1,2, and 3

# Lightbulbs	Mean Power (W)	Mean Power Std. Dev. (W)	Duration (s)	Average Energy (kJ)
0	19.3	8.69	289	5.58
1	80.8	7.74	727	58.74
2	140.7	7.94	197	27.72
3	198	8.64	318	62.96
4	251.4	9.54	93	23.38
5	307.2	8.30	88	27.03
6	361.6	9.70	89	32.18
7	415	9.32	108	44.82
8	464.9	11.50	149	69.27
9	511.6	12.80	146	74.69
10	556.2	11.92	335	186.33
11	611.5	9.81	27	16.51
12	655.6	16.03	31	20.32
13	701.1	13.14	28	19.63
14	743.7	17.17	32	23.80
15	784.4	15.38	30	23.53
16	824.9	16.54	29	23.92
17	868	16.78	124	107.63
18	908.4	17.79	222	201.66
Total Value			3062	1049.72

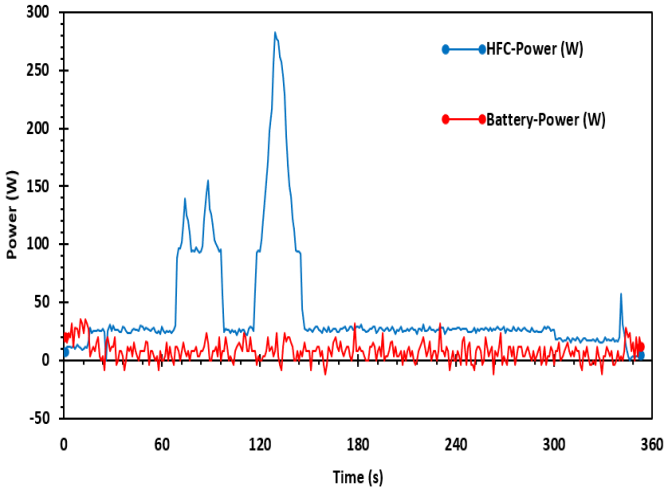

Figure 8. Power Delivered to Hexa-copter by HFC & Batteries in Motor Spinning Test

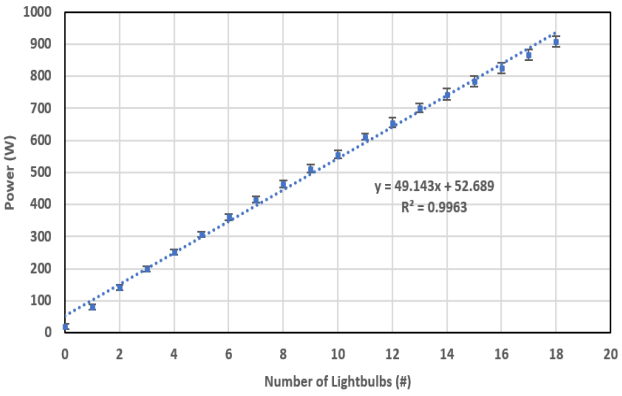

Figure 9. Combined Average Power Supplied by HFC for all three lightbulb tests

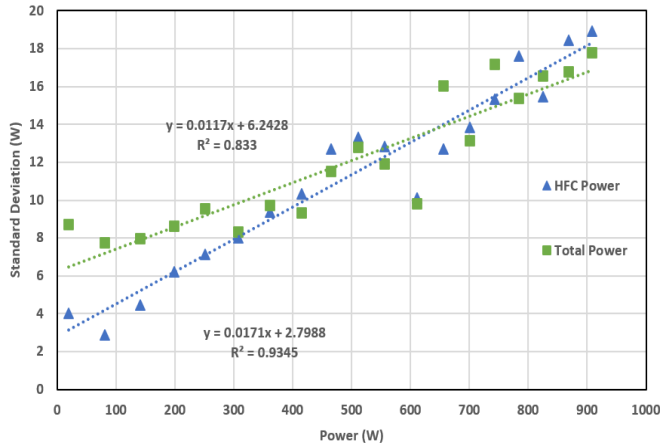

Figure 10. Standard Deviation of Mean Power Supply

The relatively wide right hand side gap between the lines in Figure 10 shows that the batteries compensated for the power supplied during the beginning period and when the power demand was on the higher end. It is likely that there exists an optimal power load for which the integrated system will be dependent on the HFC for the entirety of the test. Although, more rigorous testing is required to precisely obtain that information. The lag between the fuel cell and the battery was barely noticeable (< 1 s); this can be seen in Figure 5, Figure 6, and Figure 7 at 1125, 975, and 480 seconds respectively (see arrows), where the fuel cell ran out of hydrogen, and the batteries started in less than a second of delay. Regarding the results from the spinning test of the motors utilizing the HFC, Figure 8 demonstrates the power supplied to the drone by the HFC and the batteries with respect to time. The power contributions from the batteries in the beginning and towards the end were not negligible, which is most likely due to the battery providing energy to the fuel cell during its start-up and shut-down sequences, as seen from the surges in seconds 12 and 350 from Figure 8, respectively. Although during the test the HFC was the dominant energy source for the drone, there were few momentary power spikes from the batteries. While the exact interaction between the HFC and the batteries are not completely understood at this time, the system seems capable of seamless delivery of power without any discernible lag. Finally, from figures 4, 5, 6, and 7 an increase in the variance

of power can be seen as the load rises. The trend is more explicitly shown in the error bars from Figure 9 and in the direct increase of the standard deviation in Figure 10. Figure 11 shows the current-voltage (IV) and current-power (IP) curves for the HFC/stack on Test 3. The left vertical axis indicates the stack voltage, and it is related to the blue and grey markers. On the other hand, the yellow and orange markers are related to the HFC/stack power output on the right vertical axis. It is important to mention that the grey and yellow markers are the data points generated by the HFC manufacturing company H3 Dynamics LLC provided to compare the data points obtained by the performed tests [9]. From this graph, it is possible to observe how the stack voltage starts at around 60 V and gradually decreases as the current increases. This trend seems to flatten out when the stack current reaches 15 A. Although there seems to be noise in the IV curve, the shape of the data closely resembles that of the desired curve, as shown by the grey "H3 Dyn IV" markers. The IP curve closely follows a linear trend that correlates of the data obtained by the fuel cell manufacturing company. However, the deviation between the two curves becomes more apparent for higher current magnitudes. Even though the average difference is less than 7% on average, one of the reasons both lines are slightly different can be because of the conditions their experiment was carried out, such as different loads, battery systems, and even temperature conditions. Despite this, it is possible to assert that the data obtained is truly close to that of H3 Dynamics LLC.

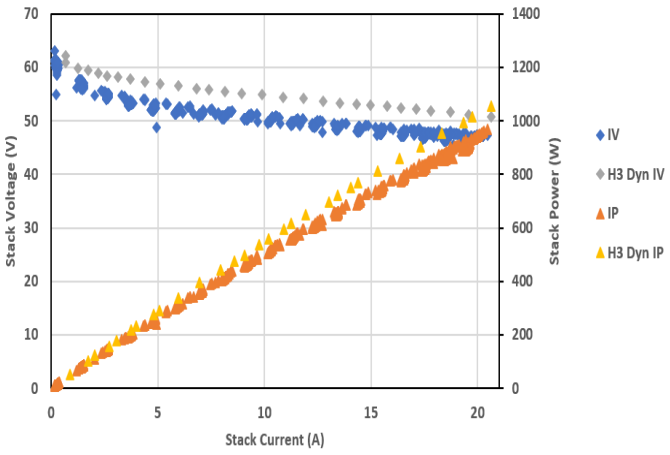

Figure 11. Test 3 HFC Current-Voltage (IV) and Current-Power (IP) Curve [9]

Finally, the temperature inside the HFC stack during Test 3 was recorded as a function of time for all four sensors. The HFC power output during this run was also included to easily relate the relation between power drawn and temperature. It is essential to mention that the data where the HFC was inactive (after the hydrogen ran out) was not included. In Figure 12 it is possible to observe that from 0-115 seconds the temperatures T1, T2, T3, and T4 within the HFC rises from 25 C° (room temperature) to 34 C° despite the power output staying the same. This may be because the even though the fuel cell is not outputting a lot of power, only about 15 W, this still generates heat, especially after being turned on. From 115-150 seconds it is possible to observe an increase in all four temperatures going from 34-37 C°, this happened clearly because the first lightbulb was turned on. Between 150-400 seconds the temperatures T2, T3, and T4 seemed to stagnate, except for T1, which decreased. This stagnation can be explained by looking at Figure 13, which shows how at 150 seconds the HFC internal fans increased their intensity and were able to keep the stack temperature the same.

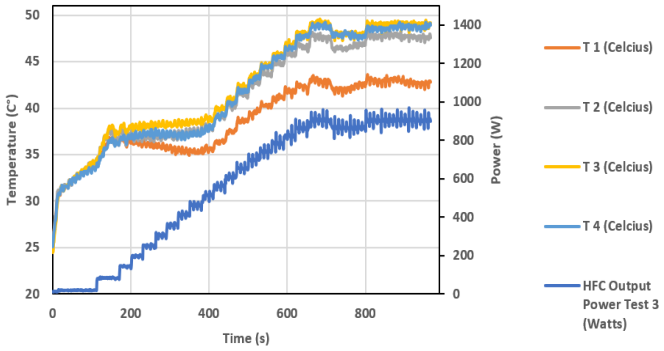

Figure 12. Stack Temperature and Power for Test 3

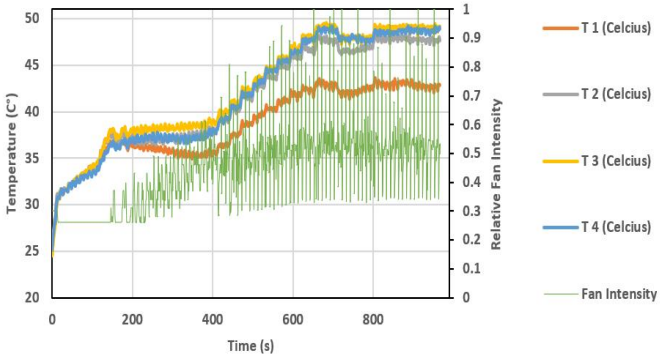

Figure 13. Stack Temperature and Fan Intensity for Test 3

However, because the power output was simultaneously increasing due to the load requirements put on the HFC, the fan intensity stagnated at ~55%, with high variability ranging from 34-100% at about 400 s. From this data, it is possible to infer that the average fan intensity was capped at this value (55%) to avoid putting a high workload on the internal fans, thus resulting on a steady increase in the stack temperature from 38 C° at 400 to 48 C° at 670 s, except for T1 which from 35 C° to 42 C° in the same time span. After the 670 seconds mark was achieved the temperatures T2, T3, and T4 stayed essentially the same mostly because the power required by the fuel cell also remained consistent (all 18 lightbulbs were on). It is even possible to observe how the temperatures T2, T3, and T4 followed the HFC power output at the 720 seconds mark, when one lightbulb was turned off for 100 seconds and the 3 temperatures suddenly dropped. Finally, the divergence shown by T1, can be explained by the location of its sensor, which could be in a different part of the fuel cell than the other three. Therefore, it can be stated that the fans play an important role in regulating HFC heat management and that their intensity may have been capped at 55%. Additionally, the T1 sensor can be in a place within the fuel cell that is away from the main center of the stack where most of the heat is produced.

5. Conclusion

In conclusion, the battery response delay is almost negligible (< 1 s). Additionally, an increase in the variation of the power supplied is directly proportional to the load in the system. This fact proves how both sources supply energy into

the system. It was also found that the battery reduces this variation for higher loads. Furthermore, the percentage of power supplied by the batteries plays an important role when turning the fuel cell on or off. The hydrogen energy density was determined to be 32.5 kJ/g. It is suspected that the deviation from the true value may be due to the efficiency of the fuel cell (~56%) and using the time as well as the power values when the battery was turned on. It was found that the IV and IP curves closely resembled those achieved by the fuel cell manufacturer with just under 7% of the average difference. It was also determined that the fans play an important role in the HFC cooling system but that their maximum performance could have been capped at 55% to maintain a longer lifespan. In terms of temperature, it was found that 3 of the 4 sensors in the fuel cell reported similar readings while the remaining one significantly diverged. This deviation can be explained by the location of said sensor, which if farther away from the stack center, the temperature readings will essentially be lower. The current work and testing mentioned above have shown great promise in terms of utilizing hydrogen and hybrid systems for drone flights. That said, this research is still a work-in-progress and several facets of it, such as- maximum achievable flight duration and comparison with battery-operated drones, its autonomous capability, payload capacity, economic feasibility, and diversification of its applications, are to be gradually explored through more laboratory and field testing.

Acknowledgment
The authors would like to thank the Arkansas Space Grant Consortium (NASA ASGC) and the higher administration of Arkansas Tech University (ATU) for their valuable support.

Ethical issue
The authors are aware of and comply with best practices in publication ethics, specifically with regard to authorship (avoidance of guest authorship), dual submission, manipulation of figures, competing interests, and compliance with policies on research ethics. The authors adhere to publication requirements that the submitted work is original and has not been published elsewhere in any language.

Data availability statement
Datasets analyzed during the current study are available and can be given following a reasonable request from the corresponding author.

Conflict of interest
The authors declare no potential conflict of interest.

References
[1] F. Zhang, J. Maddy, Investigation of the challenges and issues of hydrogen and hydrogen fuel cell applications in aviation., (n.d.).
[2] J. Wang, R. Jia, J. Liang, C. She, Y.P. Xu, Evaluation of a small drone performance using fuel cell and battery; Constraint and mission analyzes, Energy Reports. 7 (2021). https://doi.org/10.1016/j.egyr.2021.11.225.
[3] Gerardo Urdaneta, Christopher Meyers, Lauren Elizabeth Rogalski, How do drones facilitate human life?, Future Technology . 1 (2022) 7–13.
[4] J.R. Nelson, T.H. Grubesic, The use of LiDAR versus unmanned aerial systems (UAS) to assess rooftop solar energy potential, Sustain Cities Soc. 61 (2020). https://doi.org/10.1016/j.scs.2020.102353.
[5] K.E. Swider-Lyons, J.A. Mackrell, J.A. Rodgers, G.S. Page, M. Schuette, R.O. Stroman, Hydrogen fuel cell propulsion for long endurance small UAVs, in: AIAA Centennial of Naval Aviation Forum "100 Years of Achievement and Progress," 2011. https://doi.org/10.2514/6.2011-6975.
[6] A. Savvaris, Y. Xie, K. Malandrakis, M. Lopez, A. Tsourdos, Development of a fuel cell hybrid-powered unmanned aerial vehicle, in: 24th Mediterranean Conference on Control and Automation, MED 2016, 2016. https://doi.org/10.1109/MED.2016.7536038.
[7] K.T. Møller, T.R. Jensen, E. Akiba, H. wen Li, Hydrogen - A sustainable energy carrier, Progress in Natural Science: Materials International. 27 (2017). https://doi.org/10.1016/j.pnsc.2016.12.014.
[8] H3 Dynamics, Aerostak 1000W-65 Cells Specifications & Operations: User Manual, (2021). https://www.h3dynamics.com/hydrogen-fuel-cell-systems-for-air-mobility (accessed October 31, 2022).
[9] H3 Dynamics, Aerostak 1000-HV information sheet, n.d. https://www.h3dynamics.com/_files/ugd/3029f7_47d5b9c882d643cb878d6405ed2b4430.pdf (accessed August 21, 2022).

Appendix I

Table 1. List of drone components

Part	Manufacturer	Model	Weight	Notes:
Motors	T-Motor	T-Motor U8II Lite KV100	256g x 6	Smooth control, low noise, high efficiency.
Propellers	T-Motor	T-Motor G28 x 9.2 propeller	85g x 6	28" carbon fiber propellers.
Electronic Speed Controller	T-Motor	T-Motor Flame 60A ESC	73.5g x 6	Efficient, reliable, high amperage.
Frame	Gryphon Dynamics	Gryphon Hexa 1600VX Frame	2,020g	Carbon Fiber 1600mm wheelbase, hex copter design.
Batteries	Max Amps	Max Amps 5s 3250mAh LiPo	405g x 2	Two 5 cell 3250mAh LiPo batteries wired in series.
PEM Fuel Cell	H3 Dynamics	HES Aerostak A-1000 (HV)	2,131g	1kW proton exchange membrane hydrogen fuel cell in parallel with a 10 cell LiPo battery.
Hydrogen Tank	H3 Dynamics	HES F3 3L 300bar Hydrogen Tank	1,360g	3L carbon fiber construction tank.
Flight Controller	Cube Pilot	Cube Orange	73g	Fast highly powerful H7 processor with build in redundancies.
Carrier Board	Cube Pilot	Kore Carrier Board	250g	Lightweight carrier board that gives easy access to all pins of the cube orange.
Ground Station	Ardupilot	Mission Planner	N/A	Used to setup and control flight controller.